Successive neutron alignments in the yrast, negative-parity band of oblate-deformed ^{199}Tl

Saket Suman [1], S. K. Tandel [1,2,*], S. G. Wahid [1,†], Manu T. [1], M. Hemalatha,[3] B. Maheshwari [4], A. K. Jain [5],
P. Chowdhury,[2] R. V. F. Janssens [6,7], F. G. Kondev [8], M. P. Carpenter [8], T. Lauritsen [8], and D. Seweryniak[8]

[1]*School of Physical Sciences, UM-DAE Centre for Excellence in Basic Sciences, University of Mumbai, Mumbai 400098, India*
[2]*Department of Physics, University of Massachusetts Lowell, Lowell, Massachusetts 01854, USA*
[3]*Department of Physics, University of Mumbai, Mumbai 400098, India*
[4]*Department of Physics, Faculty of Science, University of Zagreb, HR-10000 Zagreb, Croatia*
[5]*Amity Institute of Nuclear Science and Technology, Amity University UP, 201313 Noida, India*
[6]*Department of Physics and Astronomy, University of North Carolina at Chapel Hill, Chapel Hill, North Carolina 27599, USA*
[7]*Triangle Universities Nuclear Laboratory, Duke University, Durham, North Carolina 27708, USA*
[8]*Argonne National Laboratory, Argonne, Illinois 60439, USA*

The negative-parity band structure built on the proton $h_{9/2}$ state in ^{199}Tl has been established up to an excitation energy of 7 MeV and spin of $(51/2)\hbar$. The level scheme has been extended with the inclusion of fourteen new transitions de-exciting levels at high spin. The $\Delta I = 1$ γ rays are found to be more prominently visible in the spectra when comparing to $\Delta I = 2$ transitions. Rotation alignments are evident at frequencies of 0.22 and 0.30 MeV with both being attributed to the breaking of pairs of neutrons in the $i_{13/2}$ subshell. Since ^{199}Tl is expected to have weak oblate deformation, and lies in a transitional region where competing contributions to the spin are expected from collective rotation and the angular momentum of high-j nucleons, calculations using both the principal axis cranking (PAC) and tilted axis cranking (TAC) formalisms have been performed to understand its structure. Both the PAC and TAC calculations are found to provide a satisfactory description of the evolution of excitation energies with spin. The PAC calculations give a good account of the experimental crossing frequencies and associated spins. The structure of the yrast, negative-parity band in ^{199}Tl may be primarily understood in terms of the collective rotation of a moderately deformed oblate nucleus, along with contributions to the angular momentum from two pairs of rotation-aligned $i_{13/2}$ neutrons.

I. INTRODUCTION

A diverse range of phenomena are manifested in nuclei with $Z \approx 80$–83 and $A \approx 190$–200. Shape coexistence, with the presence of prolate and oblate rotational bands, is evident in the lighter Hg ($Z = 80$), Tl ($Z = 81$), Pb ($Z = 82$), and Bi ($Z = 83$) isotopes, see, e.g., [1–4]. With increasing neutron numbers, oblate shapes are predominantly favored at low excitation energy, and in odd-A Tl isotopes with $A > 180$ rotational bands built on an unpaired proton in the $h_{9/2}$ orbital are found to be yrast [5–8]. The magnitude of the oblate deformation decreases with increasing neutron number when approaching the $N = 126$ shell closure. Despite this, it has been determined that the rotational properties of odd-A $^{185-199}$Tl are quite similar: this has been attributed to reduced neutron pair correlations for the heavier isotopes, leading to opposite and compensating effects on the moment of inertia [9]. The normal-deformed rotational bands established in

^{193,195,197,199}Tl, therefore, have many similarities [5,7,10–12]. Additionally, superdeformed bands have also been identified in ^{191,192,193,195}Tl [13–16], which highlight the role of the proton $i_{13/2}$ orbital. This region is also characterized by some of the first-identified and classic examples of magnetic rotational bands (so-called $M1$ bands) in Pb isotopes [17–19]. Such $M1$ bands have also been established in the doubly odd ^{194,196,198}Tl isotopes [6,8,20]. For isotopes of Tl with $A < 200$, apart from the states at low spin involving the occupation of the $h_{9/2}$ orbital, no isomeric levels have been established at high spin. In the case of ^{200}Tl and beyond, intrinsic excitations are found to play an increasing role in the realization of states at higher excitation. Recent work by this collaboration and by other groups has led to the identification of many isomers up to high spin, some of which are quite long lived, with half-lives up to hundreds of microseconds [21–25]. In all of the excitation mechanisms mentioned above, high-j orbitals (proton $h_{9/2}$, $h_{11/2}$, $i_{13/2}$, and neutron $i_{13/2}$) are found to have an important influence on the structure, whether involving rotation alignment due to the Coriolis force, the realization of magnetic rotation, the appearance of superdeformed bands, or the presence of isomeric states. Furthermore, possible chiral bands have been identified in ^{194,195,198}Tl [26–28]. The multitude of phenomena which are realized through the varying

*Corresponding author: sujit.tandel@cbs.ac.in,
sktandel@gmail.com

†Present address: Department of Physics, University of Massachusetts Lowell, Lowell, MA 01854, USA.

degrees of competition between intrinsic and collective excitations makes this region particularly interesting for nuclear structure investigations.

The isomeric $9/2^-$ state in ^{199}Tl, with $T_{1/2} = 28.4(2)$ ms [29], on which the yrast, negative-parity sequence is built, was first identified through reactions of energetic α particles on a thick ^{197}Au target [30]. Subsequent work led to the identification of a band structure built on the $9/2^-$ state [31]. More recent work, using the ^{196}Pt(^{7}Li, $4n$) reaction led to a significant extension of the level scheme up to an excitation energy of 4 MeV and a spin, $I = (33/2)\hbar$ [10]. Most of the reported levels up to 3.3 MeV were confirmed in a subsequent work using the ^{197}Au(^{4}He, $2n$) reaction, and several new nonyrast levels were also established [11]. Due to the inaccessibility of ^{199}Tl through fusion-evaporation reactions with even heavier ion beams, high-spin levels could not be identified thus far. In the present work, multinucleon transfer reactions with heavy and highly energetic beams were used to populate states up to high spin in ^{199}Tl, herewith enabling the exploration of the mechanisms responsible for nuclear structure in this excitation domain.

II. EXPERIMENT AND RESULTS

Levels at considerably higher spin, as compared to those observed in the previous work using lighter-ion ^{7}Li and α beams [10,11] were populated using $2pxn$ transfer reactions with a 1450-MeV ^{209}Bi beam from the ATLAS accelerator at Argonne National Laboratory, incident on a thick, 50 mg/cm^2, ^{197}Au target. The Gammasphere detector array comprising of 100 Compton-suppressed high-purity germanium detectors [32,33] was used to record γ-ray coincidence data. The primary focus of the analysis centered on prompt coincidence events involving the simultaneous detection of three or more γ rays in any of the Gammasphere detectors within ± 40 ns of the arrival of the pulsed beam on the target. While the delayed data, recorded >50 ns after the beam was incident on the target, were also inspected, no evidence for isomeric decays from levels above the $9/2^-$ state was found. The data were sorted into histograms with three- and four-fold coincidence events, and analyzed using the RADWARE suite of programs [34]. Matrices were constructed with γ rays detected at $90° \pm 10°$ with respect to the beam direction on one axis, and those detected at $30°/150° \pm 10°$ on the other, to enable the determination of directional correlation of γ rays de-exciting oriented states (DCO) ratios for assigning the multipole order of the transitions. However, no information on DCO ratios beyond that reported in the previous works [10,11] could be obtained.

The present work has yielded new information on high-spin levels in ^{199}Tl, specifically in the yrast, negative-parity sequence built on the $9/2^-$, 28.4(2) ms isomeric state. The extended level scheme of ^{199}Tl is presented in Fig. 1. In previous work [10], levels up to spin $I = (33/2)\hbar$ had been identified. The present data agree for all of the transitions, and their respective placements, in the $9/2^-$ band identified by Li *et al.* [10], but not with all the placements of Bhattacharya *et al.* [11]. The 619-keV, $(33/2^-) \rightarrow (29/2^-)$ γ ray is newly identified. There had been no levels identified
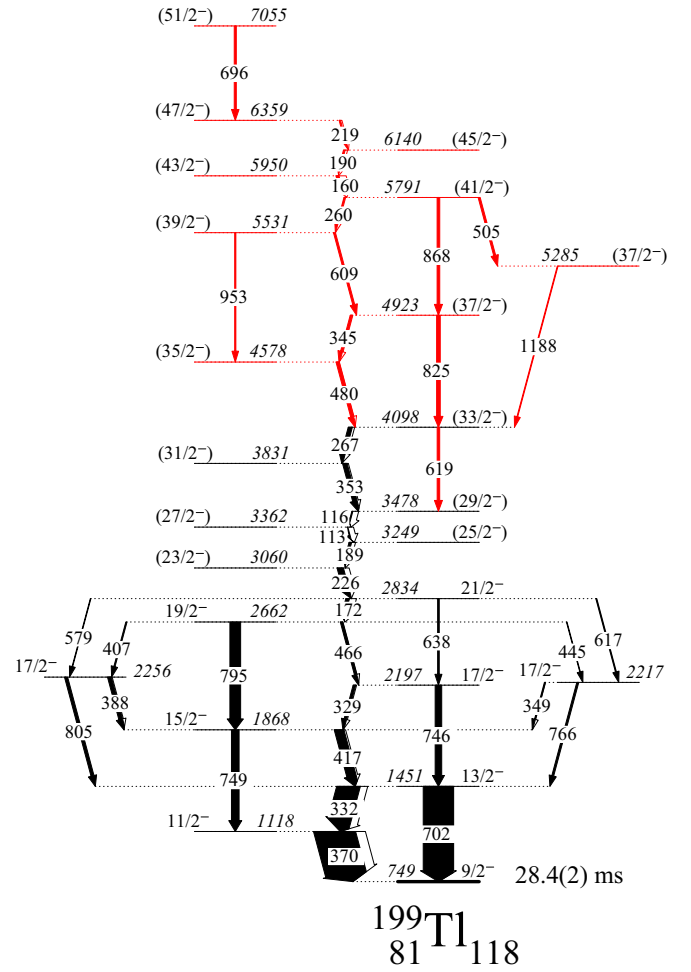

FIG. 1. Partial decay scheme of ^{199}Tl illustrating the yrast, negative-parity band structure. The transitions marked in red are the newly established ones.

in previous work above the $(33/2^-)$ level. In the present work, the yrast sequence has been extended up to the $I^\pi = (51/2^-)$ state at 7055 keV. The cascade of $\Delta I = 1$ transitions with energies 480, 345, 609, 260, 160, 190, and 219 keV is newly established. The crossover $\Delta I = 2$ transitions of energy 825 and 868 keV, and a parallel 1188-505 keV sequence between the $(33/2^-)$ and $(41/2^-)$ levels, are also identified from the present work. Additionally, the 953-keV, $(39/2^-) \rightarrow (35/2^-)$ and 696-keV, $(51/2^-) \rightarrow (47/2^-)$ transitions are newly placed. Detailed information on the levels and their assigned spin-parity, on the γ rays and their intensities is presented in Table I. All the newly identified γ rays are displayed in Figs. 2 and 3, wherein coincidence gates have been placed on several combinations of two previously established transitions below the $(33/2^-)$ level. The intensities of a few of the lower-energy, $E2$ transitions are below the observational limit, given the available statistics in the present data. This is, however, consistent with the inferred branching ratios for the $\Delta I = 1$ and $\Delta I = 2$ transitions, where the $E2$ transition energies are higher, and so are the associated transition strengths, and the γ rays are, therefore, visible.

TABLE I. Energies and intensities of γ rays, and excitation energies and spins of the associated initial and final levels in ^{199}Tl. Statistical uncertainties on γ-ray energies and intensities are listed.

E_γ (keV)	E_i (keV)	$\rightarrow$	E_f (keV)	I_i^π	$\rightarrow$	I_f^π	I_γ
112.6(2)	3361.6	$\rightarrow$	3249.0	$(27/2^-)$	$\rightarrow$	$(25/2^-)$	2.1(3)
116.4(2)	3478.0	$\rightarrow$	3361.6	$(29/2^-)$	$\rightarrow$	$(27/2^-)$	2.4(4)
159.5(1)	5950.2	$\rightarrow$	5790.7	$(43/2^-)$	$\rightarrow$	$(41/2^-)$	7.2(7)
172.1(1)	2834.4	$\rightarrow$	2662.3	$21/2^-$	$\rightarrow$	$19/2^-$	8.7(8)
188.6(2)	3249.0	$\rightarrow$	3060.4	$(25/2^-)$	$\rightarrow$	$(23/2^-)$	6.3(5)
189.6(2)	6139.8	$\rightarrow$	5950.2	$(45/2^-)$	$\rightarrow$	$(43/2^-)$	4.0(4)
219.3(1)	6359.1	$\rightarrow$	6139.8	$(47/2^-)$	$\rightarrow$	$(45/2^-)$	3.4(4)
226.0(1)	3060.4	$\rightarrow$	2834.4	$(23/2^-)$	$\rightarrow$	$21/2^-$	15.2(11)
259.5(2)	5790.7	$\rightarrow$	5531.3	$(41/2^-)$	$\rightarrow$	$(39/2^-)$	2.5(3)
266.6(1)	4097.5	$\rightarrow$	3830.9	$(33/2^-)$	$\rightarrow$	$(31/2^-)$	9.8(8)
328.9(1)	2196.8	$\rightarrow$	1867.7	$17/2^-$	$\rightarrow$	$15/2^-$	6.3(6)
332.4(1)	1450.9	$\rightarrow$	1118.5	$13/2^-$	$\rightarrow$	$11/2^-$	56.3(6)
345.2(1)	4922.8	$\rightarrow$	4577.9	$(37/2^-)$	$\rightarrow$	$(35/2^-)$	4.9(5)
349.4(2)	2217.1	$\rightarrow$	1867.7	$17/2^-$	$\rightarrow$	$15/2^-$	2.2(3)
352.9(1)	3830.9	$\rightarrow$	3478.0	$(31/2^-)$	$\rightarrow$	$(29/2^-)$	11.0(9)
369.6(1)	1118.5	$\rightarrow$	748.9	$11/2^-$	$\rightarrow$	$9/2^-$	100.0(6)
388.4(1)	2256.1	$\rightarrow$	1867.7	$17/2^-$	$\rightarrow$	$15/2^-$	9.3(6)
406.6(2)	2662.3	$\rightarrow$	2256.1	$19/2^-$	$\rightarrow$	$17/2^-$	2.4(3)
416.8(1)	1867.7	$\rightarrow$	1450.9	$15/2^-$	$\rightarrow$	$13/2^-$	23.2(10)
445.1(2)	2662.3	$\rightarrow$	2217.1	$19/2^-$	$\rightarrow$	$17/2^-$	1.2(2)
465.8(1)	2662.3	$\rightarrow$	2196.8	$19/2^-$	$\rightarrow$	$17/2^-$	5.6(6)
480.4(1)	4577.9	$\rightarrow$	4097.5	$(35/2^-)$	$\rightarrow$	$(33/2^-)$	7.2(7)
505.4(1)	5790.7	$\rightarrow$	5285.2	$(41/2^-)$	$\rightarrow$	$(37/2^-)$	4.8(5)
578.6(2)	2834.4	$\rightarrow$	2256.1	$21/2^-$	$\rightarrow$	$17/2^-$	1.4(2)
608.6(1)	5531.3	$\rightarrow$	4922.8	$(39/2^-)$	$\rightarrow$	$(37/2^-)$	4.5(5)
617.3(2)	2834.4	$\rightarrow$	2217.1	$21/2^-$	$\rightarrow$	$17/2^-$	2.3(3)
619.3(1)	4097.5	$\rightarrow$	3478.0	$(33/2^-)$	$\rightarrow$	$(29/2^-)$	6.1(6)
638.0(1)	2834.4	$\rightarrow$	2196.8	$21/2^-$	$\rightarrow$	$17/2^-$	3.9(5)
695.7(1)	7054.8	$\rightarrow$	6359.1	$(51/2^-)$	$\rightarrow$	$(47/2^-)$	5.0(6)
702.0(1)	1450.9	$\rightarrow$	748.9	$13/2^-$	$\rightarrow$	$9/2^-$	73.8(52)
745.9(1)	2196.8	$\rightarrow$	1450.9	$17/2^-$	$\rightarrow$	$13/2^-$	15.9(14)
749.1(1)	1867.7	$\rightarrow$	1118.5	$15/2^-$	$\rightarrow$	$11/2^-$	18.5(6)
766.4(1)	2217.1	$\rightarrow$	1450.9	$17/2^-$	$\rightarrow$	$13/2^-$	4.6(5)
794.6(1)	2662.3	$\rightarrow$	1867.7	$19/2^-$	$\rightarrow$	$15/2^-$	26.1(10)
805.4(1)	2256.1	$\rightarrow$	1450.9	$17/2^-$	$\rightarrow$	$13/2^-$	7.4(8)
825.3(1)	4922.8	$\rightarrow$	4097.5	$(37/2^-)$	$\rightarrow$	$(33/2^-)$	8.9(9)
867.9(1)	5790.7	$\rightarrow$	4922.8	$(41/2^-)$	$\rightarrow$	$(37/2^-)$	6.4(8)
953.4(2)	5531.3	$\rightarrow$	4577.9	$(39/2^-)$	$\rightarrow$	$(35/2^-)$	2.8(4)
1187.7(2)	5285.2	$\rightarrow$	4097.5	$(37/2^-)$	$\rightarrow$	$(33/2^-)$	1.8(3)

The spin-parity assignments above the $I^\pi = (33/2^-)$ level are tentative in the absence of significant angular correlation or distribution data for the new γ rays. However, the observation of parallel sequences above the existing $\Delta I = 1$ and $\Delta I = 2$ structures suggest $M1$ and $E2$ multipolarity, respectively. An alternative $E1/E2$ assignment for the $\Delta I = 1$ and $\Delta I = 2$ sequences is very likely ruled out by the absence of significant octupole correlations. Since all the newly established levels have half-lives below 2 ns, $M2$ multipolarity is excluded for the $\Delta I = 2$ transitions. In addition to the 260-, 505-, and 868-keV decay branches from the level at 5791 keV, there is feeding from this level and the one at 5285 keV to a positive-parity sideband built on the $15/2^+$ state [10]. In the present work, this sideband could not be extended beyond
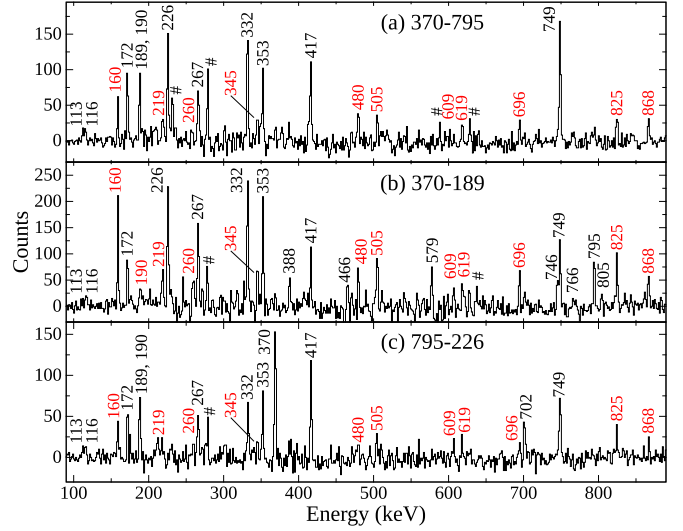

FIG. 2. Spectra with gates on two γ rays illustrating coincidence relationships with the (a) 370–795, (b) 370–189, and (c) 795–226 keV transitions which had been placed in earlier work [10]. The newly established γ rays from this work are marked in red. The hash marks indicate contaminant lines from other reaction channels.

what was reported earlier. In fact, in the present work, as yrast levels were preferentially populated, all the sidebands reported earlier [10,11] are relatively weakly fed at high spin although some lower-spin transitions, like the 629-keV γ ray de-exciting the $15/2^+$ state at 2080 keV [10], and feeding the $13/2^-$ level in the yrast band, are prominently visible in the present data.
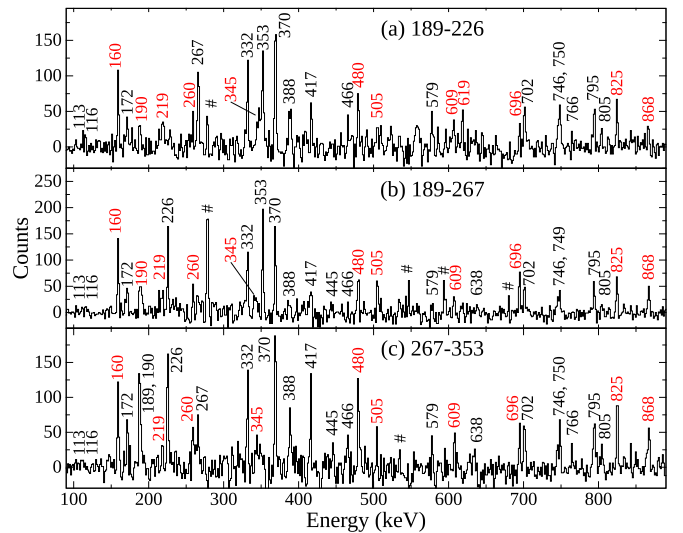

FIG. 3. Spectra with gates on two γ rays illustrating coincidence relationships with the previously placed (a) 189–226, (b) 189–267, and (c) 267–353 keV transitions [10]. New γ rays established in the present work are marked in red. The hash marks indicate contaminant lines from other reaction channels.
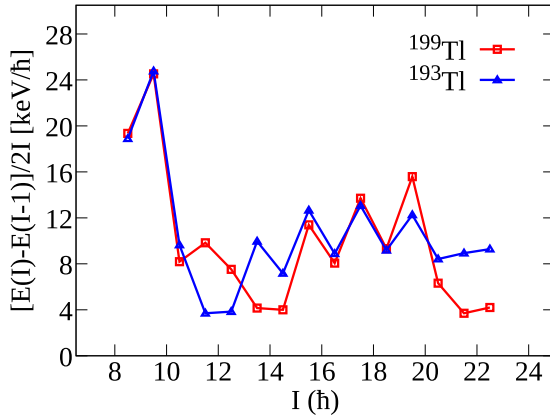
FIG. 4. Signature splitting in the band built on the $9/2^-$ state in ^{199}Tl (red). Data for ^{193}Tl [5,12] are illustrated for comparison (blue). Details are given in the text.
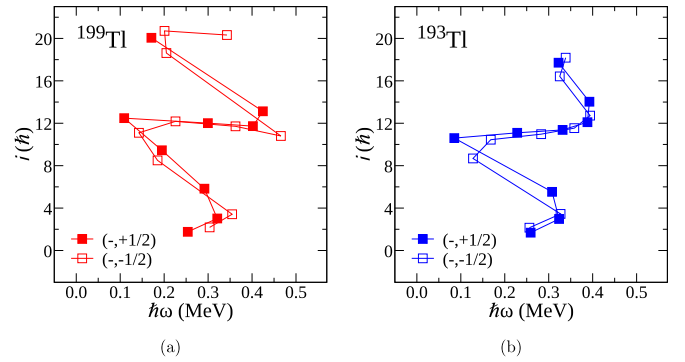

FIG. 5. Aligned angular momentum as a function of rotational frequency for the bands built on the $9/2^-$ states in (a) ^{199}Tl and (b) ^{193}Tl. The Harris parameters [47] for the reference rotor have been chosen to be $J_0 = 8\hbar^2$ MeV^{-1} and $J_1 = 40\hbar^4$ MeV^{-3} [10]. The first and second crossing frequencies in ^{199}Tl are 0.22 MeV and 0.30 MeV, respectively, while the corresponding values in ^{193}Tl are 0.26 MeV and 0.38 MeV. Possible reasons for these differences are discussed in the text.

III. DISCUSSION

Rotational bands in odd-A Tl isotopes spanning several mass numbers exhibit similar properties for reasons associated with decreasing deformation and neutron pair correlations with increasing mass number, as mentioned earlier [9]. Among the isotopes with $A \geqslant 191$, prior to this work, only the yrast, negative-parity sequence in ^{193}Tl had been observed to display two discontinuities arising from rotation alignment [5,12]. In the case of ^{199}Tl, only one instance of rotation alignment had been identified through earlier work where levels up to $(33/2^-)$ were determined [10]. With levels up to $(51/2^-)$ established from the present work, a second alignment is now evident in ^{199}Tl as well. The yrast, negative-parity sequences in ^{193}Tl and ^{199}Tl are, therefore, compared below.

The staggering in energies of the levels in the favored and unfavored signature partners of the sequences built on the $9/2^-$ states in ^{193}Tl and ^{199}Tl are displayed in Fig. 4. The trend of signature dependence is virtually identical up to the $21/2^-$ level. Above this $21/2^-$ state, the magnitude of the signature splitting is small, and the pattern of staggering is quite similar in the two cases, though the absolute values are different near the $(23/2^-)$ and $(43/2^-)$ levels. An inversion in the staggering trend is visible in the two cases at both locations where there are discontinuous changes in the excitation energy as a function of spin, owing to the rotation alignment of nucleons discussed below.

The first rotation alignment in the $h_{9/2}$ band of ^{199}Tl had been clearly delineated in the earlier work, and in the present one, the second discontinuity has also been established. The aligned angular momentum as a function of rotational frequency for ^{199}Tl is illustrated in Fig. 5(a). It is evident that the first alignment occurs at a rotational frequency, $\hbar\omega = 0.22$ MeV and is associated with a gain in aligned angular momentum of about $10\hbar$. The second alignment is visible at $\hbar\omega = 0.30$ MeV and is associated with about $8\hbar$ of gain. The corresponding frequencies in ^{193}Tl (0.26 MeV for the first, and 0.38 MeV for the second alignment), as illustrated in Fig. 5(b), are significantly higher than those in ^{199}Tl, though both crossings are postulated to have a similar character in

the two nuclei. A possible reason for this difference could be that, for the oblate deformations in both instances, orbitals from the $i_{13/2}$ subshell with lower- and higher-Ω (projection of the intrinsic angular momentum along the symmetry axis) values are involved for ^{199}Tl ($N = 118$) and ^{193}Tl ($N = 112$), respectively. For lower (higher) Ω values, the orbitals would be expected to cross the Fermi level at lesser (greater) rotational frequencies, thus accounting for the difference in the two cases. A factor which may play a role in the delayed second crossing in ^{193}Tl is the known subshell gap at $N = 110$ [35].

A. Principal axis cranking calculations

Cranking calculations were performed using the modified oscillator potential and the standard Nilsson parameters in the ultimate cranker (UC) code [36]. In this case, the cranking was performed about an axis perpendicular to the symmetry axis [principal axis cranking (PAC)] in contrast to a tilted axis as described in the next subsection. The proton and neutron pair-gap energies were obtained from experimental masses [37] following the procedure described in Ref. [38]. The total energy surface calculations for ^{199}Tl, illustrated in Fig. 6, indicate a moderately deformed oblate minimum with corresponding deformation parameters $\epsilon_2 = 0.106$ and $\gamma = -65°$ for the $I^\pi = 21/2^-$ state in the favored signature partner of the yrast, negative-parity band. The parameters ϵ_2 and γ correspond to the quadrupole deformation and triaxiality. This oblate minimum is found to persist up to the $I^\pi = 41/2^-$ state which is characterized by $(\epsilon_2, \gamma) = (0.112, -67°)$. Beyond this level, the band is driven to further negative values of γ with $(\epsilon_2, \gamma) = (0.113, -80°)$ for the $I^\pi = 45/2^-$ state, indicating a transition towards triaxial noncollective shapes. This may be correlated with the observation that no transitions could be placed in the associated band, beyond the $I^\pi = (51/2^-)$ level (see Fig. 1).
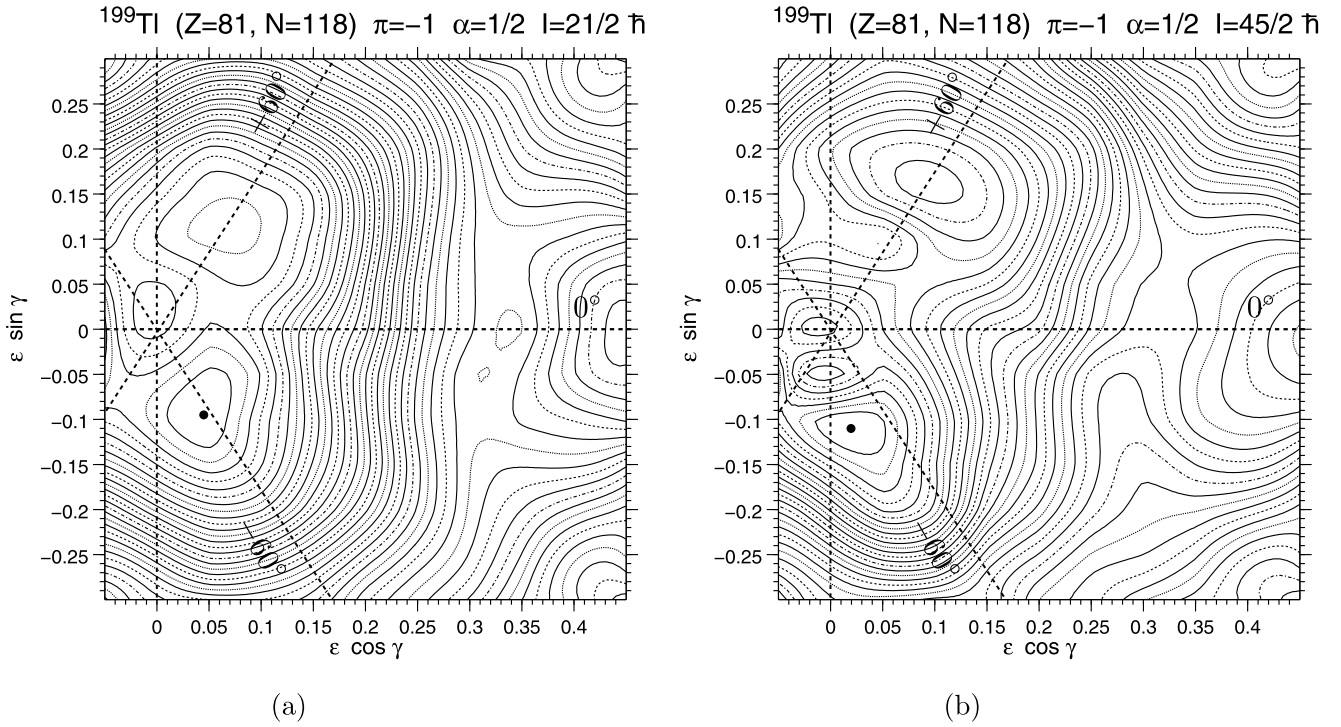
(a)   (b)

FIG. 6. Total energy surface plots illustrating energy minima in the negative-parity, yrast structure in ^{199}Tl obtained using the UC code [36]. (a) The lowest energy minimum is at $\epsilon_2 = 0.106$ and $\gamma = -65°$ for $I = 21/2\hbar$, and (b) at $\epsilon_2 = 0.113$ and $\gamma = -80°$ for $I = 45/2\hbar$.

The neutron and proton quasiparticle (qp) levels for ^{199}Tl calculated at oblate deformation are depicted in Fig. 7, and

indicate that the first neutron alignment in the $h_{9/2}$ band should be assigned to the $i_{13/2}$ AB crossing at $\hbar\omega = 0.18$ MeV, with
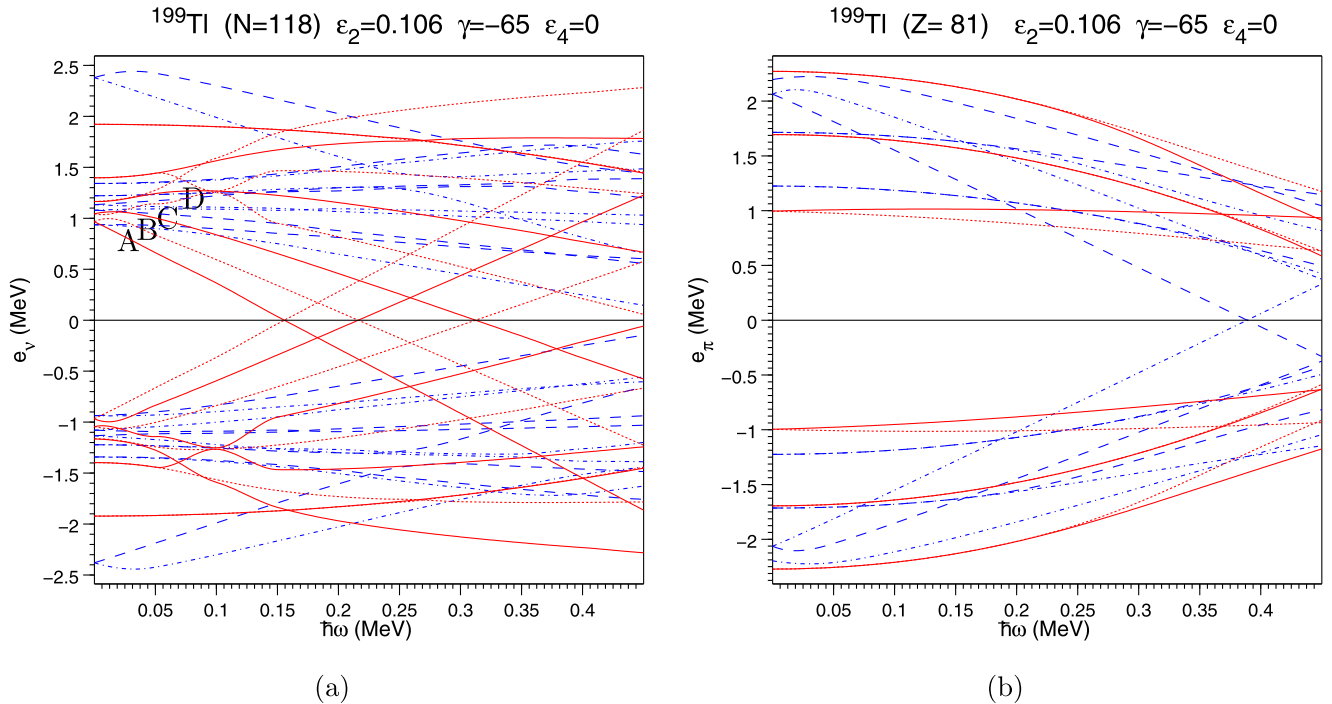

(a)   (b)

FIG. 7. (a) Neutron and (b) Proton quasiparticle energy levels for oblate deformation ($\epsilon_2 = 0.106$ and $\gamma = -65°$) in ^{199}Tl as a function of the rotational frequency, calculated using the UC code [36]. The following (standard) convention is used for labeling the orbitals (lines) with different parity (π) and signature (α): (π, α) = (+, +1/2) (solid lines); (π, α) = (+, −1/2) (short-dashed lines); (π, α) = (−, +1/2) (dot-dashed lines); (π, α) = (−, −1/2) (long-dashed lines).
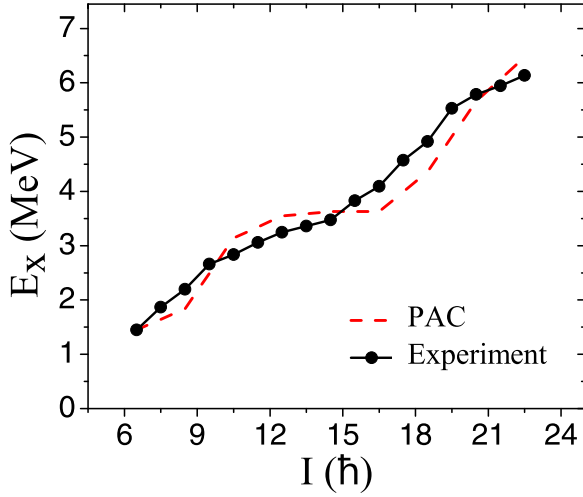
FIG. 8. Excitation energy as a function of spin from the experimental data compared with the PAC calculations. Details are provided in the text.
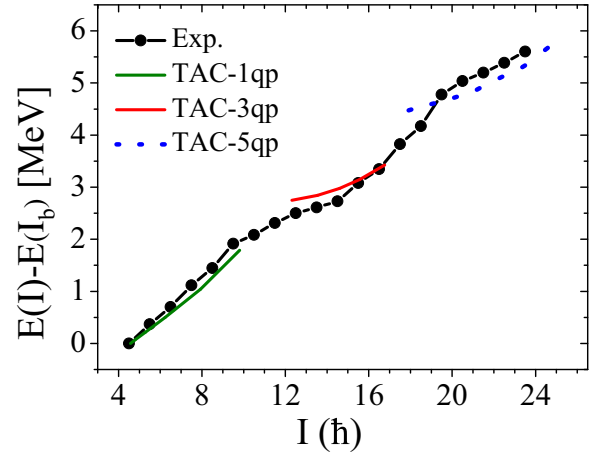

FIG. 9. A comparison of experimental energies in the yrast, negative-parity sequence with those from TAC calculations. $E(I_b)$ represents the excitation energy of the bandhead with $I = 9/2\hbar$.

the letters corresponding to the standard convention in the cranking description [39]. This prediction is in good agreement with the experimentally observed alignment at $\hbar\omega = 0.22$ MeV. The second neutron crossing is visible at $\hbar\omega = 0.32$ MeV while the first proton $h_{11/2}$ crossing is apparent only beyond 0.40 MeV (Fig. 7). The experimentally observed alignment at $\hbar\omega = 0.30$ MeV is then likely correlated with the neutron $i_{13/2}$ CD crossing. The calculated alignment gains are $12\hbar$ and $8\hbar$ for the first and second crossings, respectively.

The above calculations give a satisfactory description of the excitation energies in the yrast, negative-parity sequence from low to high spin, as illustrated in Fig. 8. The calculated energy has been normalized to that of the $13/2^-$ level from experiment to enable a comparison of the evolution of energies as a function of spin. Though the value of spin, at which the discontinuities (on account of rotation alignment) in energy are visible, is slightly overestimated by the calculations, the overall trend is well reproduced. The above considerations, viz., the agreement between experiment and PAC calculations of both rotation alignment frequencies, alignment gains, and total energies, indicate that the data are reasonably well described in terms of the rotation of the nucleus perpendicular to the symmetry axis of a moderately-deformed oblate nucleus.

B. Tilted axis cranking calculations

These calculations have been performed based on the hybrid version of the tilted axis cranking (TAC) model [40–42]. The latter combines the most optimized form of the single-particle Woods-Saxon and the modified oscillator (Nilsson) potentials. Here, the single-particle energies of the spherical Woods-Saxon potential are combined with the deformed part of the anisotropic oscillator. This approximation enables the use of a realistic flat-bottom potential, while taking into account in a simple way, the coupling between the oscillator shells [43]. Since pairing is evidently an important parameter in these calculations, we have computed proton and neutron pairing gap energies Δ_p and Δ_n from the four-point formula

using the expression given in Ref. [39]. Assuming that the pairing is reduced for the excited configurations, an attenuation factor of 0.8 has been used. The values of the neutron and proton pair gap energies used for the calculations are $\Delta_n = 0.516$ MeV and $\Delta_p = 0.792$ MeV, respectively, i.e., 80% of the odd-even mass difference. The shape parameters follow the Lund convention (ϵ_2, γ) [44].

For the band built on the one-quasiparticle, $\pi(h_{9/2})^{-1}$ configuration, the energy minimization as a function of deformation parameters gives self-consistency at values of $\epsilon_2 = -0.114$, $\epsilon_4 = 0.014$, $\gamma = 0°$, and a tilted angle $\theta = 80°$. The sequence of magnetic dipole transitions in ^{199}Tl above the $19/2^-$ level is assigned a three-qp, $\pi(h_{9/2})^{-1} \otimes \nu(i_{13/2})^{-2}$ configuration. The TAC calculations for this 3-qp configuration give a minimum in total energy at a deformation of $\epsilon_2 = -0.119$, $\epsilon_4 = 0.020$, $\gamma = 4°$, and a tilted angle $\theta = 80°$. For higher spins, another neutron pair in the $i_{13/2}$ subshell is broken, leading to the 5-qp, $\pi(h_{9/2})^{-1} \otimes \nu(i_{13/2})^{-4}$ configuration. The TAC calculations for this 5-qp configuration give a minimum in the total energy at a deformation of $\epsilon_2 = -0.094$, $\epsilon_4 = 0.013$, $\gamma = 0°$, and a tilted angle $\theta = 80°$. Additionally, calculations were performed for another 5-qp, $\pi(h_{9/2})^{-1} \otimes \nu(i_{13/2})^{-2}(j^-)^{-2}$ configuration, with $j^- \equiv h_{9/2}$ or $f_{7/2}$. This results in an energy minimum at a deformation $\epsilon_2 = -0.108$, $\epsilon_4 = 0.020$, $\gamma = 12°$, and a tilted angle $\theta = 80°$. The energies for the former configuration agree better with the experimental values, indicating that the 5-qp, $\pi(h_{9/2})^{-1} \otimes \nu(i_{13/2})^{-4}$ one is probably responsible for the observed band structure at the highest spins. The calculated 5-qp energies are compared with experiment in Fig. 9, with the 3-qp energies being renormalized to those from experiment; the 1-qp energies are also displayed. The nature of both the band crossings in the PAC and TAC calculations is the same, and the overall agreement of the two with the experimental data may be understood in terms of the relatively large tilted angle (80°) in the latter instance, which arises from the preference for angles closer to 90°, of the $i_{13/2}$ neutrons which occupy low-Ω orbitals for $N = 118$ at oblate deformation [45]. Since

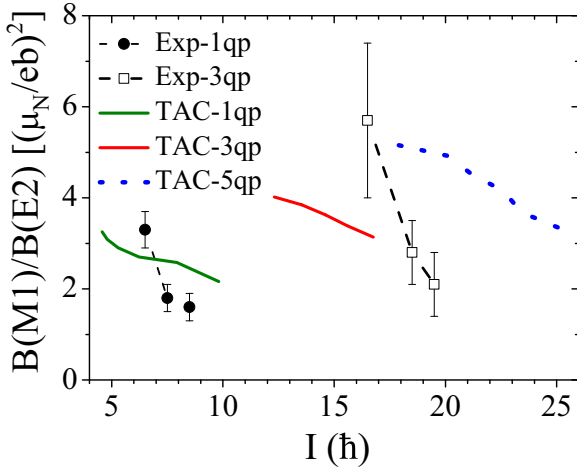FIG. 10. Ratios of reduced transition probabilities $B(M1)/B(E2)$ as a function of spin (I). The data points are the experimental values which are connected by dashed lines to guide the eye. The solid and dotted (red, blue, and green) lines represent the results of TAC calculations described in the text.

there is a considerable amount of aligned angular momentum at relatively low rotational frequencies in ^{199}Tl, there may be some limitations in the TAC description [46].

C. Branching ratios

Further insight into the nature of the observed band structures can be obtained from an inspection of the experimental ratios of magnetic dipole ($M1$) and electric quadrupole ($E2$) reduced transition probabilities: $B(M1)/B(E2)$ as a function of spin. In this region, most of the $\Delta I = 1$ transitions are found to have almost pure $M1$ character [5–8]. Due to the absence of visible $E2$ transitions de-exciting several levels, and in some cases multiple $E2$ decay branches from a given state, it was possible to obtain from the data $B(M1)/B(E2)$ values for only six levels, as displayed in Fig. 10. The $B(M1)/B(E2)$ values have been obtained using the expression

$$\frac{B(M1)}{B(E2)} = 0.697 \frac{I_\gamma(M1)E_\gamma^5(E2)}{I_\gamma(E2)E_\gamma^3(M1)}, \qquad (1)$$

where the energy (E_γ) is in MeV and I_γ represents the γ-ray intensity. The corresponding values for the 1-, 3-, and 5-qp configurations from the TAC calculations, viz., $\pi(h_{9/2})^{-1}$, $\pi(h_{9/2})^{-1} \otimes \nu(i_{13/2})^{-2}$, and $\pi(h_{9/2})^{-1} \otimes \nu(i_{13/2})^{-4}$, respectively, are also indicated. While the calculated and experimental values for the 1-qp configuration are reasonably similar, the agreement at high spins with the three values available from experiment is quite poor. The experimental $B(M1)/B(E2)$ values at high spin correspond to levels which are in the vicinity of the crossing of the 3- and 5-qp bands as a result of which they are not characteristic of purely one or the other configuration, unlike in the case of the TAC calculations. Secondly, in the crossing region, it is likely that there are

significant changes in the magnitude of the quadrupole deformation and triaxiality. These considerations may possibly be responsible for the poor agreement between the experimental $B(M1)/B(E2)$ values and the TAC results at high spin.

IV. SUMMARY

The yrast, negative-parity sequence in ^{199}Tl has been extended from the $I^\pi = (33/2^-)$ level at $\approx$4 MeV up to the $I^\pi = (51/2^-)$ state at $\approx$7 MeV, using multinucleon transfer reactions. The high-fold coincidence data recorded with the Gammasphere detector array allowed for establishing fourteen new transitions above the previously identified $(29/2^-)$ level. Two sharp backbends are visible at $I \approx 19/2\hbar$ and $39/2\hbar$, corresponding to rotational frequencies of 0.22 and 0.30 MeV, respectively. These are associated with the breaking of two pairs of $i_{13/2}$ neutrons, based on the results of PAC calculations performed using the UC code, and also those using the TAC formalism. The change in excitation energy as a function of spin is reasonably reproduced by both the PAC and TAC calculations. The $B(M1)/B(E2)$ values for the aligned structures have been inferred from the TAC calculations. The trends in signature splitting in the yrast, negative-parity bands of ^{199}Tl and ^{193}Tl are found to be similar, with the band crossing frequencies in the latter being significantly higher. Two successive rotation alignments of $i_{13/2}$ neutrons appear to be responsible for the bulk of the angular momentum generation at high spins in ^{199}Tl.

[1] J. D. Cole, A. V. Ramayya, J. H. Hamilton, H. Kawakami, B. van Nooijen, and W. G. Nettles, L. L. Riedinger, F. E. Turner, C. R. Bingham, H. K. Carter *et al.*, Phys. Rev. C **16**, 2010 (1977).

[2] S. K. Chamoli, P. Joshi, R. Kumar, R. P. Singh, S. Muralithar, R. K. Bhowmik, and I. M. Govil, Phys. Rev. C **75**, 054323 (2007).

[3] A. N. Andreyev, M. Huyse, P. Van Duppen, L. Weissman, D. Ackermann, J. Gerl, F. P. Heßberger, S. Hofmann, A. Kleinböhl, G. Münzenberg *et al.*, Nature (London) **405**, 430 (2000).

[4] A. Herzán, S. Juutinen, K. Auranen, T. Grahn, P. T. Greenlees, K. Hauschild, U. Jakobsson, R. Julin, S. Ketelhut, M. Leino *et al.*, Phys. Rev. C **96**, 014301 (2017).

[5] W. Reviol, M. P. Carpenter, U. Garg, R. V. F. Janssens, I. Ahmad, I. G. Bearden, Ph. Benet, P. J. Daly, M. W. Drigert, P. B. Fernandez *et al.*, Nucl. Phys. A **548**, 331 (1992).

[6] H. Pai, G. Mukherjee, S. Bhattacharyya, M. R. Gohil, T. Bhattacharjee, C. Bhattacharya, R. Palit, S. Saha, J. Sethi, T. Trivedi *et al.*, Phys. Rev. C **85**, 064313 (2012).

[7] R. M. Lieder, A. Neskakis, M. Müller-Veggian, Y. Gono, C. Mayer-Böricke, S. Beshai, K. Fransson, C. G. Linden, and Th. Lindblad, Nucl. Phys. A **299**, 255 (1978).

[8] A. J. Kreiner, M. Fenzl, and W. Kutschera, Nucl. Phys. A **308**, 147 (1978).

[9] J. A. Bounds, C. R. Bingham, P. Juncar, H. K. Carter, G. A. Leander, R. L. Mlekodaj, E. H. Spejewski, and W. M. Fairbank, Jr., Phys. Rev. Lett. **55**, 2269 (1985).

[10] C. B. Li, X. G. Wu, Y. Zheng, Y. J. Jin, H. L. Ma, G. S. Li, J. Zhong, B. J. Zhu, T. X. Li, Y. X. Gao *et al.*, Phys. Rev. C **97**, 034331 (2018).

[11] S. Bhattacharya, S. Bhattacharyya, R. Banik, S. Das Gupta, G. Mukherjee, A. Dhal, S. S. Alam, Md. A. Asgar, T. Roy, A. Saha *et al.*, Phys. Rev. C **98**, 044311 (2018).

[12] J. Ndayishimye, E. A. Lawrie, O. Shirinda, J. L. Easton, J. J. Lawrie, S. M. Wyngaardt, R. A. Bark, T. D. Bucher, S. P. Bvumbi, T. R. S. Dinoko, P. Jones, N. Y. Kheswa, S. N. T. Majola, P. L. Masiteng, D. Negi, J. N. Orce, J. F. Sharpey-Schafer, and M. Wiedeking, Phys. Rev. C **100**, 014313 (2019).

[13] S. Pilotte, C. H. Yu, H. Q. Jin, J. M. Lewis, L. L. Riedinger, Y. Liang, R. V. F. Janssens, M. P. Carpenter, T. L. Khoo, T. Lauritsen, F. Soramel, I. G. Bearden, C. Baktash, J. D. Garrett, N. R. Johnson, I. Y. Lee, and F. K. McGowan, Phys. Rev. C **49**, 718 (1994).

[14] Y. Liang, M. P. Carpenter, R. V. F. Janssens, I. Ahmad, R. G. Henry, T. L. Khoo, T. Lauritsen, F. Soramel, S. Pilotte, J. M. Lewis *et al.*, Phys. Rev. C **46**, R2136 (1992).

[15] P. B. Fernandez, M. P. Carpenter, R. V. F. Janssens, I. Ahmad, E. F. Moore, T. L. Khoo, F. Scarlassara, I. G. Bearden, Ph. Benet, P. J. Daly *et al.*, Nucl. Phys. A **517**, 386 (1990).

[16] J. Duprat, F. Azaiez, C. Bourgeois, J. F. Sharpey-Schafer, M. G. Porquet, M. Aïche, C. W. Beausang, R. M. Clark, I. Deloncle, R. Duffait *et al.*, Phys. Lett. B **341**, 6 (1994).

[17] A. Görgen, N. Nenoff, H. Hübel, G. Baldsiefen, J. A. Becker, A. P. Byrne, S. Chmel, R. M. Clark, M. A. Deleplanque, R. M. Diamond *et al.*, Nucl. Phys. A **683**, 108 (2001).

[18] A. K. Singh, N. Nenoff, D. Roßbach, A. Görgen, S. Chmel, F. Azaiez, A. Astier, D. Bazzacco, M. Belleguic, S. Bouneau *et al.*, Nucl. Phys. A **707**, 3 (2002).

[19] H. Hübel, Prog. Part. Nucl. Phys. **54**, 1 (2005).

[20] H. Pai, G. Mukherjee, S. Bhattacharya, C. Bhattacharya, S. Bhattacharyya, T. Bhattacharjee, S. Chanda, S. Rajbanshi, A. Goswami, M. R. Gohil *et al.*, Phys. Rev. C **88**, 064302 (2013).

[21] R. Broda, K. H. Maier, B. Fornal, J. Wrzesiński, B. Szpak, M. P. Carpenter, R. V. F. Janssens, W. Królas, T. Pawlat, and S. Zhu, Phys. Rev. C **84**, 014330 (2011).

[22] S. G. Wahid, S. K. Tandel, S. Suman, M. Hemalatha, A. Patel, P. Roy, A. Y. Deo, Pragati, P. C. Srivastava, B. Bhoy *et al.*, Phys. Rev. C **102**, 024329 (2020).

[23] P. Roy, S. K. Tandel, S. Suman, P. Chowdhury, R. V. F. Janssens, M. P. Carpenter, T. L. Khoo, F. G. Kondev, T. Lauritsen, C. J. Lister *et al.*, Phys. Rev. C **100**, 024320 (2019).

[24] V. Bothe, S. K. Tandel, S. G. Wahid, P. C. Srivastava, Bharati Bhoy, P. Chowdhury, R. V. F. Janssens, F. G. Kondev, M. P. Carpenter, T. Lauritsen *et al.*, Phys. Rev. C **105**, 044327 (2022).

[25] J. Wrzesiński, R. Broda, B. Fornal, W. Królas, T. Pawlat, M. P. Carpenter, R. V. F. Janssens, D. Seweryniak, S. Lunardi, C. A. Ur *et al.*, Eur. Phys. J. A **20**, 57 (2003).

[26] P. L. Masiteng, E. A. Lawrie, T. M. Ramashidzha, R. A. Bark, B. G. Carlsson, J. J. Lawrie, R. Lindsay, F. Komati, J. Kau, P. Maine *et al.*, Phys. Lett. B **719**, 83 (2013).

[27] T. Roy, G. Mukherjee, Md. A. Asgar, S. Bhattacharyya, Soumik Bhattacharya, C. Bhattacharya, S. Bhattacharya, T. K. Ghosh, K. Banerjee, S. Kundu *et al.*, Phys. Lett. B **782**, 768 (2018).

[28] E. A. Lawrie, P. A. Vymers, J. J. Lawrie, Ch. Vieu, R. A. Bark, R. Lindsay, G. K. Mabala, S. M. Maliage, P. L. Masiteng, S. M. Mullins *et al.*, Phys. Rev. C **78**, 021305(R) (2008).

[29] B. Singh, Nucl. Data Sheets **108**, 79 (2007).

[30] R. M. Diamond and F. S. Stephens, Nucl. Phys. **45**, 632 (1963).

[31] J. O. Newton, S. D. Cirilov, F. S. Stephens, and R. M. Diamond, Nucl. Phys. A **148**, 593 (1970).

[32] I.-Y. Lee, Nucl. Phys. A **520**, c641 (1990).

[33] R. V. F. Janssens and F. S. Stephens, Nucl. Phys. News **6**, 9 (1996).

[34] D. C. Radford, Nucl. Instrum. Methods Phys. Res. A **361**, 297 (1995).

[35] E. Ngijoi-Yogo, S. K. Tandel, G. Mukherjee, I. Shestakova, P. Chowdhury, C. Y. Wu, D. Cline, A. B. Hayes, R. Teng, R. M. Clark, P. Fallon *et al.*, Phys. Rev. C **75**, 034305 (2007).

[36] T. Bengtsson, Nucl. Phys. A **512**, 124 (1990).

[37] F. G. Kondev, M. Wang, W. J. Huang, S. Naimi, and G. Audi, Chin. Phys. C **45**, 030001 (2021).

[38] P. Möller and J. R. Nix, Nucl. Phys. A **536**, 20 (1992).

[39] R. Bengtsson, S. Frauendorf, and F.-R. May, At. Data Nucl. Data Tables **35**, 15 (1986).

[40] V. I. Dimitrov, F. Dönau and S. Frauendorf, Phys. Rev. C **62**, 024315 (2000).

[41] Amita, A. K. Jain, and B. Singh, At. Data Nucl. Data Tables **74**, 283 (2000).

[42] Amita, A. K. Jain, V. I. Dimitrov, and S. G. Frauendorf, Phys. Rev. C **64**, 034308 (2001).

[43] P. Agarwal, S. Kumar, S. Singh, R. K. Sinha, A. Dhal, S. Muralithar, R. P. Singh, N. Madhavan, R. Kumar, R. K. Bhowmik, S. S. Malik, S. C. Pancholi, L. Chaturvedi, H. C. Jain, and A. K. Jain, Phys. Rev. C **76**, 024321 (2007).

[44] G. Andersson, S. E. Larsson, G. Leander, P. Moller, S. G. Nilsson, I. Ragnarsson, S. Aberg, R. Bengtsson, J. Dudek, B. Nerlo-Pomorska, K. Pomorski, and Z. Szymanski, Nucl. Phys. A **268**, 205 (1976).

[45] R. M. Clark and A. O. Macchiavelli, Annu. Rev. Nucl. Part. Sci. **50**, 1 (2000).

[46] S. Frauendorf and J. Meng, Z. Phys. A: Hadrons Nucl. **356**, 263 (1996).

[47] S. M. Harris, Phys. Rev. **138**, B509 (1965).